Applied Catalysis B: Environmental 90 (2009) 330–338

Contents lists available at ScienceDirect

Applied Catalysis B: Environmental

journal homepage: www.elsevier.com/locate/apcatb

Adsorption and photocatalytic degradation of phenol and 2,4 dichlorophenoxiacetic acid by Mg–Zn–Al layered double hydroxides

Jaime S. Valente [a,b,*], Francisco Tzompantzi [c], Julia Prince [b], Jose G.H. Cortez [a], Ricardo Gomez [c]

[a] Instituto Mexicano del Petroleo, Eje Central # 152, 07730 Mexico D.F., Mexico
[b] Universidad Autonoma Metropolitana-Azcapotzalco, Quimica de Materiales, Av. San Pablo # 180, 02200 Mexico D.F., Mexico
[c] Universidad Autonoma Metropolitana-Iztapalapa, Departamento de Quimica, Av. San Rafael Atlixco # 186, 09340 Mexico D.F., Mexico

ARTICLE INFO

Article history:
Received 8 December 2008
Received in revised form 31 January 2009
Accepted 16 March 2009
Available online 25 March 2009

Keywords:
Photocatalysis
Layered double hydroxides
Phenol degradation
2,4 Dichlorophenoxiacetic acid

ABSTRACT

Mg–Zn–Al layered double hydroxides (LDHs) with varying amounts of zinc were prepared by the coprecipitation method. Solids were analyzed by XRD and N_2 physisorption, confirming the formation of pure LDH phase; and the production of mixed oxides with high specific surface areas (182–276 $m^2\ g^{-1}$) after calcination. Band gap energy was also determined, presenting the expected decreasing tendency on increasing zinc amounts. These mixed oxides were tested both for the adsorption of 2,4 dichlorophenoxiacetic acid (2,4-D) and for the photocatalytic degradation of 2,4-D and phenol. Nearly total (97%) degradation of initial 1.45 mmol L^{-1} of 2,4-D, with 1 g calcined LDH per liter, was accomplished in 9 h, while phenol half-life was as short as 3.5 h, with the catalyst with lowest zinc amount (5 wt.%). Langmuir adsorption isotherms are presented. Solids were also characterized by XRD and FTIR analysis after photocatalytic and adsorption activity, to determine the presence of 2,4-D. The versatility of LDH decomposition products in the elimination of different contaminants by different mechanisms puts them forward as a viable alternative for environmental remediation.

1. Introduction

In recent years, there has been an increasing demand for solutions to the multiple environmental problems associated with the use of toxic compounds. Amongst these, phenol and chlorinated phenols play a major role, because of their high toxicity, extensive use and their weak retention in soil sediments. Sources of phenol include waste solutions in various industries, such as petroleum refining and plastics. Chlorinated acid phenols, represented by 2,4 dichlorophenoxiacetic acid (2,4-D), are commonly used as herbicides and pesticides.

Many research efforts have been devoted to developing methods for the elimination of these compounds from soil and water by means of biological and physical–chemical methods. Amid the latter, studies on photocatalytic degradation of herbicides and phenol by UV irradiation with titanium dioxide [1–3], Fe (III) chelates [4], Fenton oxidation [5] and metal phtalocyanines [6] are worth noticing. Another important branch corresponds to the development of suitable adsorbents that may be used in the elimination of these compounds from contaminated water. Some of the adsorbents that have been studied include activated carbons [7], and, to a lesser extent, layered double hydroxides.

Layered double hydroxides (LDHs) are a class of naturally occurring anionic clays. The basic structure of an LDH may be derived from partial isomorphic substitution of divalent cations in a brucite lattice by trivalent cations, such that the layer acquires a positive charge, which is compensated for by the intercalation of anions between the layers. Since an ample assortment of compounds with the basic LDH structure might be prepared, they are represented by the general formula: $[M_{(1-x)}^{II}M_x^{III}(OH)_2]A_{x/n}^{n-}\cdot mH_2O$, where M^{II} includes: Mg^{2+}, Co^{2+}, Cu^{2+}, Ni^{2+}, Zn^{2+}, etc.; M^{III} may be Al^{3+}, Cr^{3+}, In^{3+}, Mn^{3+}, Ga^{3+}, Fe^{3+}; and A^{n-} might be any organic and/or inorganic anions. Many ternary LDHs involving mixtures of different M^{II} and/or M^{III} may also be prepared [8].

LDHs have been studied as catalysts or catalyst precursors to a great extent for the past few decades [9]. Given that the calcination products of LDHs are mixed oxides, which are solids with basic properties [10,11], they have been successfully employed in many organic reactions catalyzed by bases [12,13]. Moreover, LDHs have been employed in a wide range of technological applications, such as hybrid composites, antacid agents, flame retardants and PVC additives. In addition, several research groups worldwide have attempted to introduce biological species and organic compounds between the layers [8].

There has been considerable interest in the use of LDHs to remove negatively charged species from aqueous solution, due to

* Corresponding author at: Instituto Mexicano del Petroleo, Eje Central # 152, 07730 Mexico D.F., Mexico. Tel.: +52 55 54 53 52 88.
E-mail address: jsanchez@imp.mx (J.S. Valente).

0926-3373/$ – see front matter © 2009 Elsevier B.V. All rights reserved.
doi:10.1016/j.apcatb.2009.03.019

their high uptake capacity, which can be accounted for by their large surface area, high anion-exchange capacities, and flexible interlayer space. The anion-exchange capacity of LDHs is affected by the nature of the interlayer anions initially present and the layer charge density (*i.e.* the *x* value in the general formula). When the layer charge density is very high, the exchange reaction may become difficult. LDHs have particularly great affinity for CO_3^{2-}, so these anions are very difficult to displace in anion-exchange reactions.

LDHs can take up anion species from solution by three different mechanisms: surface adsorption, interlayer anion exchange, and reconstruction of a calcined LDH by the "memory effect" [8]. LDHs and their calcination products have been successfully employed as adsorbents for a variety of anion species and/or pollutants, such as sulfur oxides [14], sodium dodecylsulfate [15,16], synthetic dyes [17], and pesticides like MCPA [18], imazamox [19], dicamba [20] and 2,4-D [21,22].

Photochemical applications of LDHs, on the other hand, have been less widely studied. Photocatalytic activity of ZnAl LDHs with different M^{II}/M^{III} ratios was evaluated for the degradation of methyl-orange, removing up to 93% of initial 1×10^{-3} mmol L^{-1} [23]. Photodegradation of phenol has also been attempted with heat-treated and calcined ZnAl LDHs, achieving a 71% conversion of phenol (initially 0.05 mmol L^{-1}) after 120 min [24]. Other applications of LDHs in photochemistry include the controlled photodimerization of unsaturated carboxylate species intercalated in the interlayer galleries of MgAl LDHs [25], and the intercalation of organic dyes in order to improve their UV, oxygen and thermal stability [26–28].

This paper presents a study of the adsorption and photocatalytic degradation of 2,4-D and phenol by Mg–Zn–Al mixed oxides obtained by calcination of the corresponding layered double hydroxides, which appear as a promising alternative for the elimination of toxic substances from waste water. The main advantages of these materials are their easy preparation, low cost, and reusability. Calcined Mg–Al layered double hydroxides were also tested to determine the role of Zn^{2+} cations.

2. Experimental

2.1. Synthesis

The layered double hydroxides containing Mg–Al and Mg–Zn–Al with different amounts of zinc were prepared by the coprecipitation at low supersaturation method at constant pH [29]. An aqueous solution (A, 1 M) was prepared, containing the dissolved salts of $Mg(NO_3)_2{\cdot}6H_2O$, $Zn(NO_3)_2{\cdot}6H_2O$ and $Al(NO_3)_3{\cdot}9H_2O$ in the required amounts. Meanwhile, an alkaline solution (B, 2 M) was prepared, containing K_2CO_3 and KOH. Solutions (A) and (B) were added simultaneously to a glass reactor, containing previously 100 cm^3 of deionized H_2O, at a controlled pH of 9. The precipitate obtained was kept under vigorous mechanical stirring, at a temperature of 353 K for 18 h. Afterwards, the product was thoroughly washed with hot deionized water in order to eliminate excess ions, and dried at 373 K for 24 h. The M^{II}/M^{III} molar ratio was kept constant at 2 for all samples.

For instance, to prepare 100 g of a Mg–Zn–Al LDH with 15% wt. of zinc, the following amounts were used: $Mg(NO_3)_2{\cdot}6H_2O$ = 182.5 g, $Zn(NO_3)_2{\cdot}6H_2O$ = 68.13 g and $Al(NO_3)_3{\cdot}9H_2O$ = 117.7 g, dissolved in 1097.7 mL of distilled water.

Samples will be referred to as MgZnAl–X, X is the zinc wt.% content in the sample. Mg/Al-LDH will be simply called MgAl. Solids were calcined at 723 K for 5 h prior to adsorption and photocatalytic tests.

2.2. Adsorption tests

The adsorption capacity of calcined LDHs was determined by preparing 6 solutions of 2,4-D (pK_a = 2.8) [22], with concentrations varying between 0.45 and 1.58 mmol L^{-1} (100 and 350 ppm), in 200 mL of distilled water. These solutions afforded a pH ≈ 3, which was not adjusted at any point. 0.1 g of the calcined solid was added, and the solution was maintained under constant stirring. Aliquots were taken from the solutions every 30 min for 6 h.

The remaining amount of 2,4-D in solution was determined by UV–vis spectroscopy, using a Cary 100 spectrophotometer with integration sphere. Concentration of 2,4-D is directly proportional to absorbance by the Beer-Lambert law: $A = \varepsilon bC$; where A is the absorbance at 282 nm, ε is the molar absorptivity coefficient, b is the path length (0.01 m), and C is the molar concentration. A calibration curve was constructed from 0.045 to 1.8 mmol L^{-1} (10–400 ppm), obtaining a correlation coefficient r^2 = 0.9992, and a slope εb = 1669.82.

All experiments were repeated three times to verify the repeatability of the results. The adsorption of phenol by LDHs was negligible, and is thus not reported here.

2.3. Photocatalytic tests

Photodegradation of 2,4-D was carried out by preparing a solution of 1.36 mmol L^{-1} (300 ppm) in distilled water. Four aliquots of 200 mL were taken, and 0.2 g of calcined LDH was added to each one. Temperature was kept constant at 298 K, and the pH was not adjusted at any moment. The solutions were stirred in a batch reactor for 1 h to allow adsorption of contaminant into the solid. Afterwards, solutions were irradiated with UV light for 1, 3, 6 or 9 h, using a Pen Ray Power Supply lamp, 115 V, λ = 254 nm, intensity = 4400 μW cm^{-2}, light length 1(1/8) in., without filter, which was immersed in the solution.

The remaining amount of 2,4-D at a given time was determined by UV–vis spectroscopy, using a Cary 100 spectrophotometer with integration sphere, following the procedure previously explained (Section 2.2).

Photodegradation of phenol was carried out by preparing solutions of 0.42 mmol L^{-1} (40 ppm) in distilled water, and following the same procedure as described above. Solutions were irradiated with UV light for 1–5 h, using the same lamp described above. The remaining amount of phenol was determined directly from solution by UV–vis spectroscopy, using a Cary 100 spectrophotometer with integration sphere. Absorbance was measured at 269 nm. A calibration curve was constructed from 0.16 to 0.45 mmol L^{-1}, obtaining a correlation coefficient r^2 = 0.9777, and a slope εb = 1363.7.

2.4. Characterization

2.4.1. Chemical analysis

The chemical composition of solids was determined in a PerkinElmer model Optima 3200 Dual Vision by inductively coupled plasma atomic emission spectrometry (ICP-AES).

2.4.2. Textural analysis

The texture of the calcined samples (at 723 K for 5 h in air) was analyzed by N_2 adsorption–desorption at 77 K on a Quantachrome Autosorb-3B apparatus. Prior to the analysis, the samples were outgassed in a vacuum (10^{-5} Torr) at 673 K for 12 h. The surface areas were calculated by the Brunauer–Emmett–Teller (BET) method, and the pore size distribution and total pore volume were determined by the Brunauer–Joyner–Hallenda (BJH) method applied to the desorption branch.

Table 1
Chemical composition, surface area, pore volume and pore diameter values.

Sample	Chemical formula	M^{II}/M^{III}	Zinc (wt.%)	S_{BET} ($m^2\,g^{-1}$)	Pore volume ($cm^3\,g^{-1}$)	Pore diameter (nm)
MgAl	$[Mg_{0.66}\,Al_{0.34}(OH)_2](CO_3)_{0.17}{\cdot}H_2O$	1.98	–	276	0.62	18
MgZnAl-5	$[Mg_{0.61}Zn_{0.06}Al_{0.33}(OH)_2](CO_3)_{0.165}{\cdot}H_2O$	2.03	5.25	255	1.05	18
MgZnAl-10	$[Mg_{0.55}Zn_{0.12}Al_{0.33}(OH)_2](CO_3)_{0.165}{\cdot}H_2O$	2.03	10.37	182	0.84	18
MgZnAl-15	$[Mg_{0.46}Zn_{0.16}Al_{0.38}(OH)_2](CO_3)_{0.19}{\cdot}H_2O$	1.63	12.16	211	0.90	32

2.4.3. X-ray diffraction

The X-ray diffraction pattern of the samples was measured in a θ–θ Bruker D-8 Advance diffractometer with Cu Kα radiation, a graphite secondary-beam monochromator, and a scintillation detector. Diffraction intensity was measured between 4° and 80°, with a 2θ step of 0.02° and a counting time of 9 s per point.

2.4.4. Band gap energy determination

Band gap energy (E_g) was determined using a Cary 100 spectrophotometer with integration sphere, the same equipment employed for the determination of the amount of 2,4-D adsorbed by the solids.

For semiconductor materials, the relation between absorption edge and absorbance is as follows:

$$\alpha h\upsilon = B(h\upsilon - E_g)m$$

where α is the absorbance, $h\upsilon$ is the photon energy (eV), E_g is the band gap energy, and B is the characteristic constant for certain materials. For direct band gap semiconductors $m = 1/2$, whereas $m = 2$ for indirect band gap semiconductors.

The method for determining the band gap energy values is by plotting the square root of the Kubelka-Munk function multiplied by the photon energy versus the photon energy and extrapolating the linear part of the rising curve to zero. For each material, E_g was calculated in accord with the following equation:

$$E_g\,(\mathrm{eV}) = \frac{1239b}{-\alpha}$$

where α and b are coefficients which were linearized in the appropriate region of the spectrum [30–32].

2.4.5. Infrared spectroscopy

The DRIFT spectrum were recorded with a Bruker Equinox 55 spectrophotometer equipped with a Harrick diffuse reflection attachment (HDRPBR-3), at a resolution of 4 cm^{-1} and averaging over 200 scans, in the range 4000–400 cm^{-1}. Solids were placed in the sampler cup and the spectra were recorded at room temperature.

3. Results and discussion

3.1. Catalyst characterization prior to photocatalytic degradation

3.1.1. Chemical and textural analyses

LDHs chemical composition and the specific surface area of their calcination products are presented in Table 1. Even though the M^{II}/M^{III} nominal molar ratio was kept constant at 2 during the synthesis for all samples, the real molar ratios ranged from 1.63 for MgZnAl-15 to 2.03 for MgZnAl-5 and for MgZnAl-10. This fact can be attributed to an incomplete incorporation of the cations inside the layers. It is worth noticing, however, that the zinc content does not depend on this molar ratio variation, since the wt.% of zinc is 5.25, 10.37 and 12.16 for MgZnAl-5, MgZnAl-10 and MgZnAl-15, respectively.

Nitrogen adsorption–desorption isotherms of calcined samples are displayed in Fig. 1. Data was plotted in arbitrary units, showing only the shape of the isotherm and not its actual size. All samples present type IV isotherms according to IUPAC classification, which corresponds to mesoporous solids. Furthermore, hysteresis loops are type H3, indicating the presence of slit-shaped pores with non-uniform size and shape [33], created by the collapse of brucite-like sheets upon calcination.

The largest surface area, 276 $m^2\,g^{-1}$, corresponds to the solid without zinc, MgAl. Nevertheless, the compounds with zinc showed larger pore volume, reaching the maximum on MgZnAl-5, 1.05 $cm^3\,g^{-1}$. Indeed, amongst the zinc-containing samples, MgZnAl-5 presents the best textural properties, namely, the highest surface area and pore volume, see Table 1.

3.1.2. X-ray diffraction

X-ray diffraction patterns, presented in Fig. 2, reveal pure hydrotalcite-like phase in all solids. Characteristic 0 0 3 and 1 1 0 reflections around $2\theta \approx 11°$ and $2\theta \approx 60°$, respectively, correspond to basal and in-plane spacing. Unit cell parameters c and a, listed in Table 2, are obtained by Bragg's law, assuming hexagonal stacking. Also, Table 2 presents crystal sizes, which were calculated using Scherrer's equation.

Interlayer distances diminish gradually upon zinc addition. This phenomenon might be explained by an increase in layer charge density, due to the larger electronegativity of zinc compared to that of magnesium; the Allred-Rochow's electronegativities are 1.66 and 1.29, respectively. Furthermore, crystal size appears to be directly proportional to the amount of zinc, in agreement with the results obtained by textural analysis, as a higher degree of crystallinity implies a loss in surface area.

3.1.3. Band gap energy of materials

As can be appreciated in Fig. 3, the addition of zinc originates the shift of the adsorption edge to longer wavelengths, and thus a

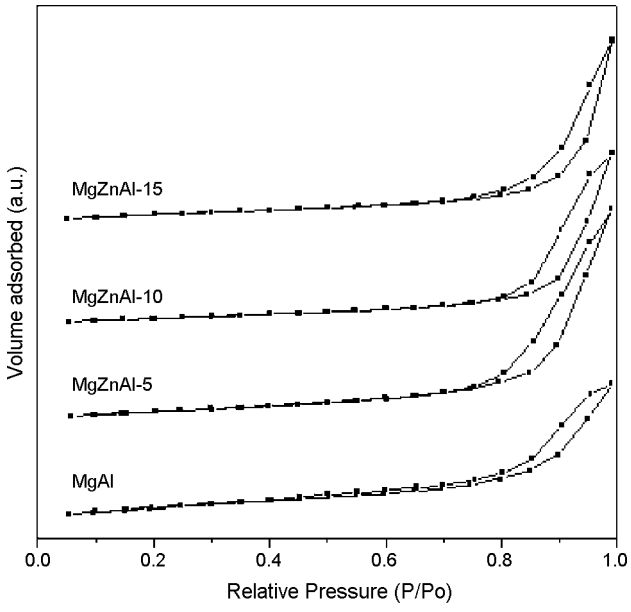

Fig. 1. N_2 adsorption–desorption isotherms of calcined solids.

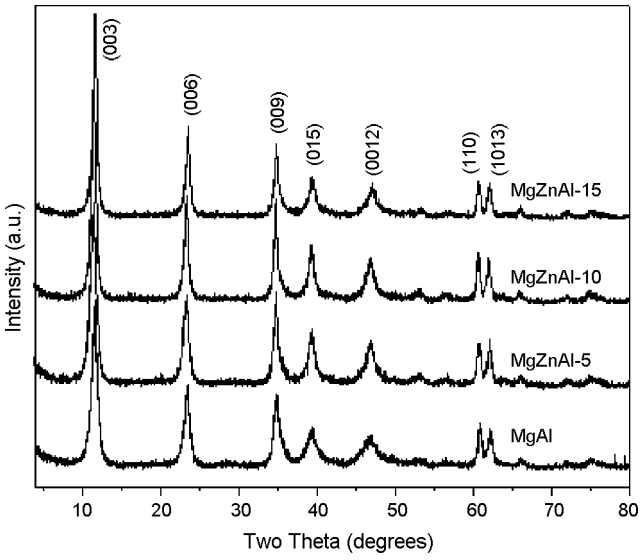

Fig. 2. XRD patterns of LDH samples.

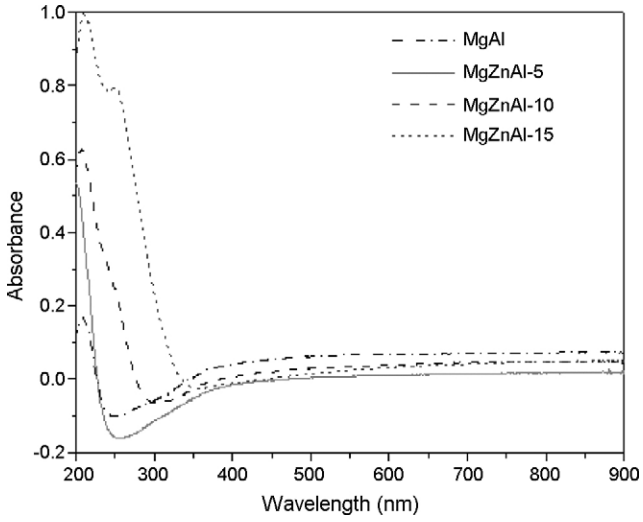

Fig. 3. UV–vis absorbance spectrum, used for the determination of band gap energy.

Table 2
Unit cell parameters and crystal sizes.

Sample	Unit cell parameters (Å)		Interlayer distance (Å)[a]	Crystal size (Å)[b]	
	c	*a*		L_{003}	L_{110}
MgAl	23.005	3.045	2.868	85	281
MgZnAl-5	22.911	3.046	2.837	88	283
MgZnAl-10	22.795	3.047	2.798	112	317
MgZnAl-15	22.711	3.044	2.770	125	398

[a] Calculated considering the thickness of the brucite lattice as 4.8 Å.
[b] Calculated using Scherrer's equation.

decrease in the band gap energy, from 5.45 eV for MgAl to 3.85 eV for MgZnAl-15. However, this is still relatively high when compared to a semiconductor material, such as anatase, which has band gap energy of 3.0–3.2 eV [3]. Band gap energy values for all samples are listed in Table 3.

3.2. Adsorption of 2,4-D by calcined LDHs

Several experiments were carried out to determine the adsorption capacity of calcined solids. 0.1 g of catalyst were used in all cases, while initial concentrations of 2,4-D were varied between 0.45 and 1.58 mmol L^{-1}. The pH was not adjusted at any point, which resulted in acidic solutions, with initial pH ≈ 3. As soon as the adsorption was begun, the pH rose until it reached a value of ≈9, which corresponds to a typical LDH dispersion. A representative example of pH evolution for a solution with 0.1 g calcined MgZnAl-5 and initial 1.36 mmol L^{-1} of 2,4-D is shown in Fig. 4. This behavior provides evidence for a rapid regeneration of LDH structure, as will be discussed later.

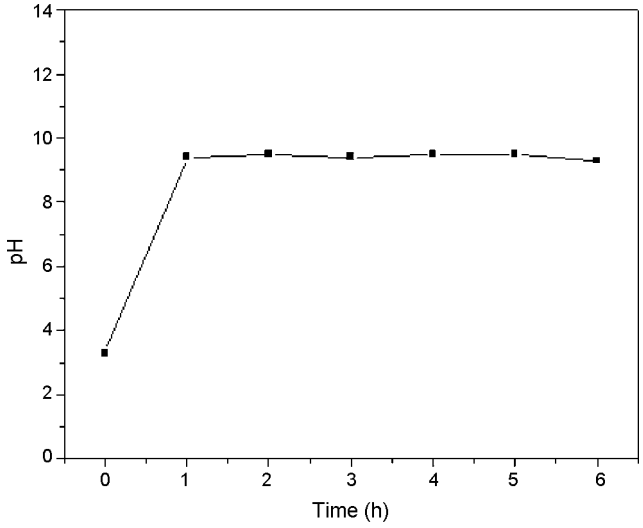

Fig. 4. Representative pH evolution as a function of time, during adsorption of 1.36 mmol L^{-1} of 2,4-D by 0.1 g of MgZnAl-5.

The remaining amount of 2,4-D was followed by UV–vis spectroscopy. Fig. 5 shows the UV spectra, in the region from 250 to 300 nm, recorded at different times for sample MgZnAl-5 with 1.36 mmol L^{-1} of 2,4-D. Notice that the gray curve (0 h) is graphed to the right *y*-axis (scaled from 0 to 2.5). The rest of the curves are graphed to the *y*-axis on the left, scaled from 0 to 0.5. This was deemed necessary for the sake of clarity, due to the huge difference in absorbance. After 0.5 h, there is a substantial decrease of 2,4-D concentration in solution; which continues to decrease up to 2 h. After this time, concentration increases gradually, owing to

Table 3
Langmuir parameters Q_m, K and linearization coefficient r^2 for the adsorption of 2,4-D by LDHs, band gap energy values, and total amounts of 2,4-D adsorbed and degraded.

Sample	Q_m (mmol g_{cat}^{-1})	K (L $mmol^{-1}$)	r^2	2,4-D/Al molar ratio[a]	Band gap energy (eV)	Total 2,4-D adsorbed[b]	Total 2,4-D degraded[c]
MgAl	1.787	8.719	0.971	0.418	5.45	62%	–
MgZnAl-5	2.827	69.541	0.999	0.650	5.43	97%	99%
MgZnAl-10	2.479	61.614	1	0.590	4.47	85%	95%
MgZnAl-15	1.322	30.562	1	0.293	3.85	46%	93%

[a] Calculated with Q_m values and data from chemical analysis.
[b] Of initial 1.45 mmol L^{-1}, with 0.1 g calcined LDH.
[c] Of initial 1.36 mmol L^{-1}, with 0.2 g calcined LDH.

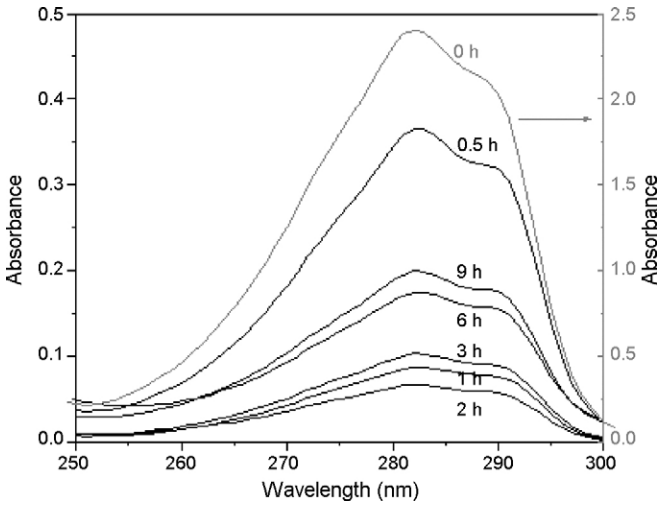

Fig. 5. UV spectra of the adsorption of 1.36 mmol L^{-1} of 2,4-D by MgZnAl-5, recorded as a function of time. Notice the 0 h curve (in gray) corresponds to the right-hand scale.

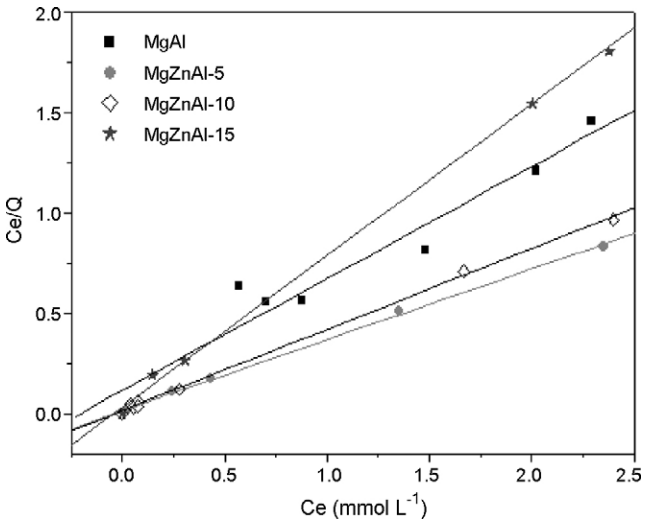

Fig. 7. Langmuir adsorption isotherms of 2,4-D onto calcined LDHs.

the establishment of a competition between 2,4-D and CO_3^{2-} from the ambient, as LDHs are known for their great affinity for CO_3^{2-}. In order to avoid this, an inert atmosphere (N_2, He, Ar) and decarbonated water should be used. However, the goal of these experiments was to keep the conditions as comparable to a natural environment as possible. This competition continues up to 9 h of adsorption, where equilibrium is established. This phenomenon was observed in all samples, and with different 2,4-D concentrations. Therefore, concentration was measured after 9 h in all cases.

Adsorption curves are presented in Fig. 6, where *Ce* is the equilibrium concentration of 2,4-D in the solution (mmol L^{-1}), and *Q* is the quantity adsorbed of 2,4-D by gram of solid. Adsorption of 2,4-D by MgAl calcined LDH resembles an *S* type isotherm, according to the classification proposed by Giles et al. [34]. On the other hand, adsorption of 2,4-D onto calcined MgZnAl LDHs may be described as an *L* type (Langmuir) adsorption isotherm.

S type isotherms are far less common than Langmuir adsorption isotherms. One of the possible explanations for an *S* curve is that the solute (2,4-D) meets strong competition for substrate sites from another species [34]; in this case, competition is established with CO_3^{2-}. This competition occurs on all solids, but is more significant on MgAl due to its higher basic strength [35]. Stronger basic sites have larger affinity for CO_3^{2-}. Charge defects induced by Zn^{2+} atoms diminish overall basic strength, and likely reduces the competition for adsorption sites.

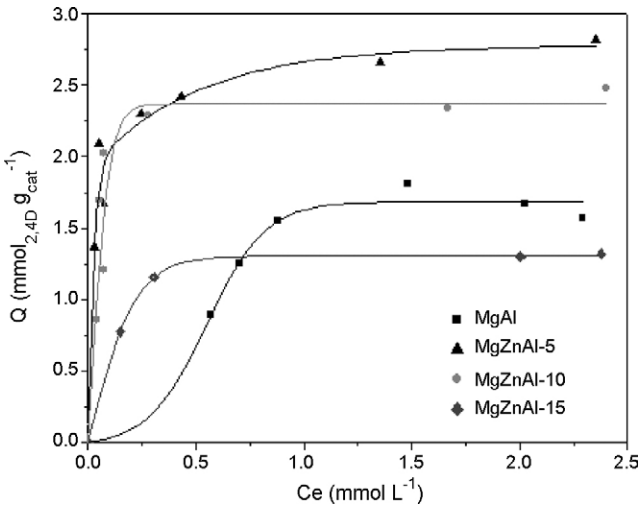

Fig. 6. Adsorption of 2,4-D by calcined LDHs.

The Langmuir model is based on the assumptions that all the adsorption sites are equivalent (*i.e.* the surface of the adsorbent is uniform); all adsorption occurs by the same mechanism; adsorbed molecules do not interact with one another, and only a monolayer is formed at the maximum adsorption. The expression for Langmuir adsorption isotherms, after applying the Langmuir linear regression, is:

$$\frac{Ce}{Q} = \frac{Ce}{Q_m} + \frac{1}{K}$$

where *Ce* is the equilibrium concentration (mmol L^{-1}), *Q* is the amount adsorbed (mmol g^{-1}), Q_m is the maximum amount adsorbed per unit mass of LDH (mmol g^{-1}), and *K* is the affinity constant. Langmuir adsorption curves are presented in Fig. 7. Langmuir parameters Q_m and *K*, along with the linearization coefficient r^2 are summarized in Table 3. Linearization coefficients show an excellent fit for all MgZnAl solids; in MgAl, the lower coefficient (0.97) is still good enough to allow comparison between Q_m parameters.

The adsorption capacity was largest for the sample with lowest zinc amount, MgZnAl-5, 2.827 mmol g_{cat}^{-1}. As the amount of zinc increases, the adsorption capacity diminishes. MgAl has a slightly larger adsorption capacity than MgZnAl-15. The fact that MgZnAl-5 presents the largest adsorption capacity may be explained by its higher pore volume and surface area. Samples MgZnAl-10 and MgZnAl-15 have very similar textural properties; nevertheless, MgZnAl-15 has the poorest adsorption capacity. These results point out that adsorption capacity is intimately related to textural properties, and also to the addition of an optimum amount of zinc.

3.3. Photodegradation of 2,4-D by calcined LDHs

The photocatalytic activity of calcined sample MgZnAl-5 is shown in Fig. 8. The total percentage of 2,4-D that was degraded is presented in Table 3, showing that in all cases, over 90% of the contaminant was degraded after 9 h. The best results were obtained for the sample with the lowest amount of zinc, which also had the largest adsorption capacity.

For all the mixed oxides tested in this study, the adsorption initially appears to be much faster than the photocatalysis; after 1 h, the remaining 2,4-D amount is smaller for adsorption, when

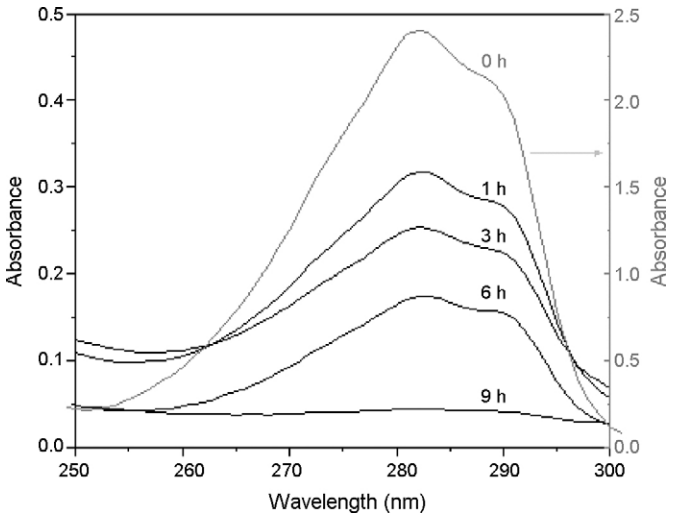

Fig. 8. Photodegradation of 2,4-D by MgZnAl-5. Notice the 0 h curve (in gray) corresponds to the right-hand scale.

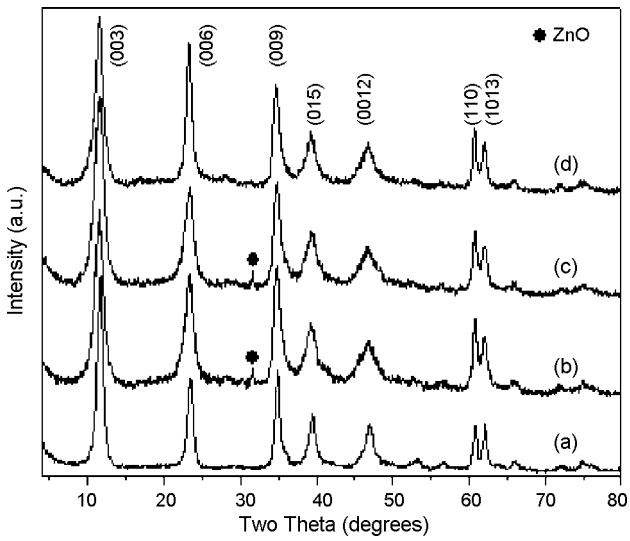

Fig. 10. XRD patterns of (a) MgZnAl-5 LDH, as-synthesized; calcined MgZnAl-5 after (b) 1 h, (c) 6 h and (d) 9 h of photocatalytic degradation of 2,4-D.

comparing any given catalyst. Fig. 9 portrays the percentage of 2,4-D removed, as a function of time, for representative sample MgZnAl-5, with initial concentration of 1.36 mmol L^{-1} (0.2 and 0.1 g of catalyst for photocatalysis and adsorption, respectively). After 1 h, 87% of 2,4-D was photodegraded; in the same time interval, 97% 2,4-D was adsorbed. Nonetheless, the adsorption curve shows a slight increase in concentration, probably due to the competition established between CO_3^{2-} and 2,4-D, as discussed previously. On the other hand, photocatalytic degradation is initially slower, but with a constant decrease in 2,4-D concentration. This decrease should be actually due to photodegradation, and not merely adsorption.

To determine if the contaminant may be directly photolyzed by UV light, another experiment was conducted, irradiating a 2,4-D solution without any catalyst. Results are depicted in Fig. 9. There appears what seems to be a small increase in 2,4-D concentration. This phenomenon may be due to some kind of modification suffered by the compound, which increases the absorbance at 282 nm. Therefore, given this result, it is reasonable to assume that 2,4-D is not photolyzed by UV light at 254 nm, and that any degradation observed is in fact due to the photocatalytic action of calcined LDHs.

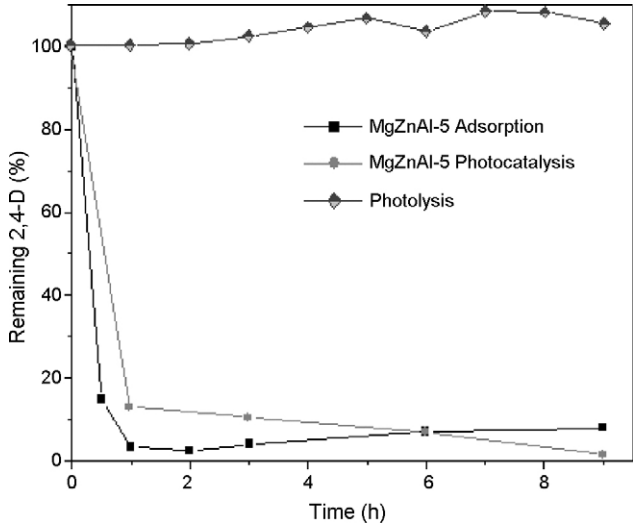

Fig. 9. Photodegradation and adsorption of 2,4-D on MgZnAl-5 as a function of time; and photolysis of 2,4-D.

These results are a significant improvement on reported degradation capacity of 2,4-D by different catalysts. For instance, it has been reported that full degradation of 0.9 mmol L^{-1} of 2,4-D can be achieved in 5 h, with 1 wt.% TiO_2 supported on HY zeolite, using 2 g of catalyst per liter of solution [36]. An hexagonal mesoporous silica modified with copper phtalocyanines has also been tested, degrading 90% of 0.05 mmol L^{-1} in 60 min, adding 1.2 wt.% H_2O_2 and 0.5 g of catalyst per liter [6].

3.4. Characterization of solids after adsorption and photocatalytic activity

3.4.1. X-ray diffraction

Fig. 10 displays the X-ray diffraction patterns of (a) the as-synthesized MgZnAl-5 LDH; and the XRD patterns of the same solid after being submitted to calcination and photocatalytic activity during (b) 1 h, (c) 6 h and (d) 9 h.

It is a well-known fact that the layered structure of LDHs collapses upon calcination, forming a mixed oxide; and that the LDH structure is recovered when put in contact with water or solution. This property of LDHs is commonly known as *memory effect* [8]. Results depicted in Fig. 10 reveal that the LDH structure is recovered after only 1 h of photocatalytic activity. However, a residual amount of the ZnO phase formed during calcination is evidenced by the appearance of a low-intensity peak at $2\theta \approx 31.7^{\circ}$ in spectra (b) and (c), samples after 1 and 6 h of photocatalysis, respectively. The presence of this impurity is explained by considering different conditions during synthesis and reconstruction, such as temperature, pH, and time. In fact, after 9 h (spectrum d), this peak is not apparent and the XRD pattern corresponds to that of a pure LDH. The same behavior was observed in the other solids and also in the adsorption tests.

Subsequent activation by thermal treatment renders once again a mixed oxide; thus, these catalysts are suitable of being reused a number of times. To this effect, a test was conducted on MgZnAl-5 catalyst; results showed that there is no loss in activity.

Even though at pH ≈ 9 (Fig. 4) 2,4-D exists as 2,4-dichlorophenoxiacetate, which could be intercalated in LDH interlayer region as charge-compensating anion, no increase in interlayer spacing was evidenced. The cell parameters of these solids are displayed in Table 4. Both c and a cell parameters show a minimal increase

Table 4
Unit cell parameters and crystal sizes for MgZnAl-5 LDH, as-synthesized, and after 1, 6 or 9 h of photocatalytic degradation of 2,4-D.

Sample	Unit cell parameters (Å)		Interlayer distance (Å)[a]	Crystal size (Å)[b]	
	c	a		L_{003}	L_{110}
MgZnAl-5	22.911	3.046	2.837	88	283
1 h photocatalysis	23.220	3.047	2.940	59	252
6 h photocatalysis	23.105	3.048	2.902	58	228
9 h photocatalysis	23.107	3.051	2.902	66	307

[a] Calculated considering the thickness of the brucite lattice as 4.8 Å.
[b] Calculated using Scherrer's equation.

when compared to the as-synthesized MgZnAl-5. This may be due to the fact that the initial 2,4-D/[Mg–Zn–Al] molar ratio is too small, 0.24 and 0.10 for adsorption and photocatalytic tests, respectively, and previous studies on intercalation of 2,4-D in ZnAl LDHs found that the 2,4-D/[Zn–Al–Cl] molar ratio must be ≥1 for an increase in interlayer distance [37]. Furthermore, at such low 2,4-D concentrations, competition for intercalation sites between 2,4-D and CO_3^{2-} from the ambient is an important factor, LDHs have greater affinity for CO_3^{2-}.

Crystal size from Scherrer's equation confirms a loss in crystallinity during reconstruction of LDHs, which is also explained by the different conditions during synthesis and reconstruction, as mentioned before.

3.4.2. Infrared spectroscopy

Results from DRIFT analysis are presented in Fig. 11. Only the region between 1800 and 600 cm^{-1} is shown, as all vibration bands assigned to 2,4-D appear in this interval. A comparison is presented between pure MgZnAl (spectrum a), and samples after adsorption (spectrum b) or after photocatalytic degradation of the 2,4-D pesticide (spectra c–f). As-synthesized MgZnAl LDHs, spectrum a in Fig. 11A–C, present a vibration band at 1650 cm^{-1}, assigned to the bending vibration of water, $\delta(H_2O)$, and a strong band in the low frequency region, corresponding to vibration modes and ascribed to M–O vibration at 995 cm^{-1} [37]. Also, a strong band at 1425 cm^{-1} indicates the presence of CO_3^{2-} anions in the interlayer region. This band is still present, though with diminished intensity, in spectrums b–f confirming the competition between CO_3^{2-} and 2,4-D for intercalation in the interlayer region of LDHs.

Characteristic bands of 2,4-D anion are present on all samples after 9 h of adsorption, see spectrums b in Fig. 11A–C. Unassigned bands that must correspond to 2,4-D appear at ∼1396 and 1107 cm^{-1}. The band at 1485 cm^{-1} has been ascribed to a stretching vibration of the C=C aromatic bond; and the deforming vibration of the C–H aromatic bond appears at 1255 cm^{-1} [38,39]. The bands at 1290 and 1070 cm^{-1} correspond to antisymmetric and symmetric vibrations of the C–O–C bonds, respectively. Furthermore, the band at ∼1612 cm^{-1} was assigned to a C=O vibration [22].

Spectrums c–f in Fig. 11A–C were taken after 1, 3, 6 and 9 h of photocatalytic degradation of 2,4-D, respectively. Upon longer UV irradiation times, the presence of 2,4-D becomes less evident, clearly indicating the photodegradation of the contaminant. After 9 h, all bands ascribed to 2,4-D are completely gone, evidencing the total degradation of the contaminant. This result supports the real photodegradation of the contaminant, as opposed to a simple adsorption.

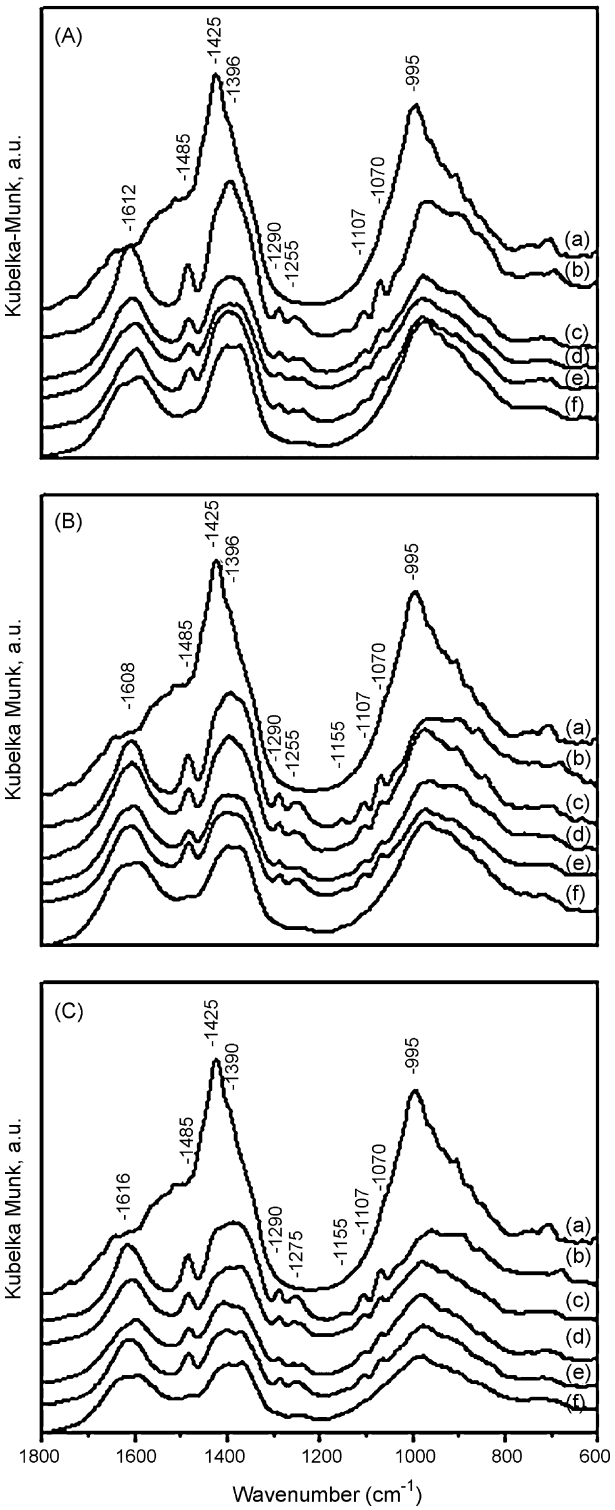

Fig. 11. DRIFT spectra of phases obtained after retention of 2,4-D on MgZnAl. (A) 5 wt.% Zn, (B) 10 wt.% Zn, (C) 15 wt.% Zn. (a) As-synthesized LDH; (b) 9 h adsorption; photodegradation stage and (c) 1 h-UV, (d) 3 h-UV, (e) 6 h-UV and (f) 9 h-UV.

3.5. Photodegradation of phenol by calcined LDHs

Photodegradation of phenol was carried out with the same method as the photodegradation of 2,4-D; with initial concentration of 0.42 mmol L^{-1}. All solutions were allowed 1 h of stirring before irradiating with UV light. As evidenced in Fig. 12, from 0 to 1 h, there is no change in phenol concentration, indicating that phenol is not adsorbed by LDHs. A strong photocatalytic activity is observed for calcined MgZnAl-5, degrading ca. 70% of phenol in 6 h.

As a comparison, a solution was irradiated with UV light without any catalyst. In this case, phenol suffered some kind of

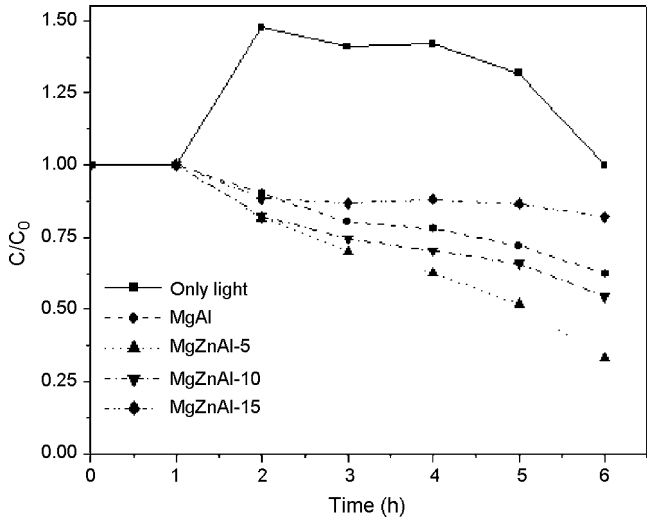

Fig. 12. Photolysis and photodegradation of phenol by calcined LDHs.

modification, which explains what seems to be an increase in concentration. Polymerization of phenol would be a suitable explanation, as it has been reported that polymerization occurs by direct photolysis under UV ($\lambda > 200$ nm) irradiation [40]. After 6 h of UV irradiation, concentration is lowered back to the initial one; therefore, phenol is not directly photolyzed by UV light at 254 nm.

The Langmuir–Hinshelwood model is commonly used to describe the kinetics of photocatalytic reactions of organic compounds in aqueous solutions. It relates the degradation rate r and the concentration of organic compound C, and is expressed as follows:

$$r = -\frac{dC}{dt} = \frac{k_r K_{ad} C}{1 + K_{ad} C}$$

where k_r is the intrinsic rate constant and K_{ad} is the adsorption equilibrium constant. When the adsorption is relatively weak and the concentration of organic compounds is low, the factor $K_{ad}C$ is insignificant, and the equation can be simplified to the first-order kinetics with an apparent rate constant ($K_{app} = k_r K_{ad}$), which gives, after integration in the interval [C, C_0]:

$$\ln \frac{C_0}{C} = K_{app} t$$

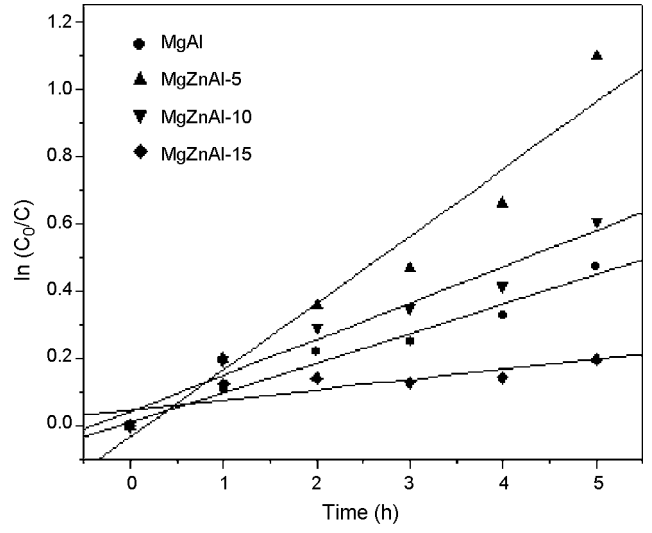

Fig. 13. Pseudo first-order kinetics degradation of phenol, by the Langmuir-Hinshelwood model.

Table 5
Apparent constant, half-life and linearization coefficient for the Langmuir-Hinshelwood model for phenol photodegradation.

Sample	K_{app}	$t_{1/2}$ (h)	r^2
MgAl	0.085	7.90	0.987
MgZnAl-5	0.199	3.47	0.972
MgZnAl-10	0.108	6.44	0.978
MgZnAl-15	0.030	23.41	0.849

Plotting of $\ln(C_0/C)$ versus reaction time t yields a straight line, where the slope is the apparent rate constant. The half-life of the degraded organic compound can then be easily calculated. Fig. 13 shows the lineal plot of phenol photodegradation, which adjusts well to a pseudo-first-order kinetic behavior. Apparent constant K_{app}, phenol half-life, and the linearization coefficient r^2 are summarized in Table 5. Phenol half-life is as short as 3.47 h, with MgZnAl-5 catalyst, and nearly 70% of initial 0.42 mmol L^{-1} is degraded after 6 h.

As a comparison, 71% of 0.05 mmol L^{-1} phenol conversion is achieved in 2 h with Zn_4Al LDHs [24]. Another study reported 94% phenol degradation in 3 h, with initial 0.51 mmol L^{-1} phenol, adding 1.77 mmol L^{-1} H_2O_2, a 1 g per liter ratio of commercial catalyst Degussa P-25 TiO_2; but required a 400 W UV lamp and constant acidic pH [2]. Thus, the catalysts presented here appear as a feasible alternative for the elimination of phenolic compounds.

Characterization of the catalysts after phenol photodegradation are not presented because phenol is not adsorbed on LDHs, and thus the XRD and FTIR results showed no differences between the original catalysts and the solids after photocatalytic activity.

3.6. Photocatalytic performance elucidation

Usually, photocatalytic processes are thought to be based on the generation of electron/hole pairs by means of band gap radiation. Larger band gap energy values indicate a diminished semiconducting capacity, and, theoretically, a reduced photocatalytic activity. In this sense, it would be expected that MgZnAl-15 be the best photocatalyst. Experimental data do not agree with this hypothesis, given the evident superiority of MgZnAl-5 as adsorbent and as photocatalyst in both reactions.

This result could be due to two factors. Firstly, the higher specific surface area and pore volume presented by MgZnAl-5 are significant, for they imply an increase of catalytically active sites. Furthermore, a smaller amount of zinc (5 wt.% versus >10 wt.%) is probably better distributed along the brucite-like layers. Recent studies using combined ^1H and ^{25}Mg MAS NMR techniques with the latest advances in instrumentation have revealed that Mg and Al distribution in LDH layers is not random; and that in Mg/Al = 2, they are ordered in what was described as a honeycomb arrangement [41]. It is not unreasonable to assume that a second divalent cation will also be uniformly distributed along LDH sheets, given that, upon calcination of LDHs, a mixed oxide is formed; of which XRD analyses show only MgO phase in MgAl and MgZnAl with low zinc content. Therefore, it is correct to suppose that ZnO is present, but in crystals that remain undetectable by XRD. With increasing zinc content a mixture of MgO and ZnO phases appear on calcined XRD patterns.

In smaller particles, the chemistry is dominated by surface atoms, because they represent a greater percentage of the total structure. These atoms on surfaces and edges are not fully coordinated, and therefore are more reactive [42]. For this reason, the catalytic activity of any given metal or metal oxide will be greater in smaller particles. Introducing more zinc in the LDH leads to the formation of larger ZnO particles upon calcination, with higher proportions of inactive bulk atoms.

4. Conclusions

This work showed that introducing a small amount of zinc in an MgAl LDH modifies substantially the band gap energy and the adsorption capacities of these materials. Adsorption capacity and photodegradation activity were tested on herbicide 2,4-D, a representative molecule of an ample variety of pollutants, using calcined LDHs. Nearly total elimination of the contaminant can be achieved either way: 97% adsorption and 99% degradation. The maximum adsorption capacity and photocatalytic activity were displayed by the solid with the lowest zinc content (~5 wt.%). This is explained partially by its improved textural properties, a larger surface area and a high pore volume (>1 g cm^{-3}). Also, the addition of an optimum amount of zinc enhanced the photocatalytic properties. Around 70% of phenol was photodegraded in 6 h over MgZnAl-5 catalyst. The photocatalytic activity displayed by these solids, particularly MgZnAl-5, is superior to previous reports on photodegradation of these contaminants. Its versatility is worth noticing, it has dual adsorption and degradation capabilities for anionic pollutants, and as well is able to degrade very stable compounds, such as phenol. Furthermore, it has the advantages of being easy to prepare, stable, economic and of working under ambient conditions. Moreover, the catalysts can be reused, after being reactivated by thermal treatment. Hence, the application of LDHs for the removal of a wide variety of aqueous contaminants may be envisaged.

Acknowledgements

This work was supported by the Instituto Mexicano del Petroleo and the Universidad Autonoma Metroplitana. J.P. gratefully acknowledges Conacyt for a graduate-school scholarship.

References

[1] V. Belessi, D. Lambropoulou, I. Konstantinou, A. Katsoulidis, P. Pomonis, D. Petridis, T. Albanis, Appl. Catal. B 73 (2007) 292.
[2] C.-H. Chiou, C.-Y. Wu, R.-S. Juang, Chem. Eng. J. 139 (2008) 322.
[3] B. Pourabbas, B. Jamshidi, Chem. Eng. J. 138 (2008) 55.
[4] C.Y. Kwan, W. Chu, Chemosphere 67 (2007) 1601.
[5] W. Chu, C.Y. Kwan, K.H. Chan, C. Chong, Chemosphere 57 (2004) 1165.
[6] E. DeOliveira, C.R. Neri, A.O. Ribeiro, V.S. Garcia, L.L. Costa, A.O. Moura, A.G.S. Prado, O.A. Serra, Y. Iamamoto, J. Colloid Interf. Sci. 323 (2008) 98.
[7] B. Ozkaya, J. Hazard. Mater. B129 (2006) 158.
[8] D.G. Evans, X. Duan, Layered Double Hydroxides. Struc. Bond., vol. 119, Springer-Verlag, Berlin, Heidelberg, Germany, 2006.
[9] F. Figueras, Top. Catal. 29 (2004) 189.
[10] J. Sanchez Valente, F. Figueras, M. Gravelle, P. Kumbhar, J. Lopez, J.P. Besse, J. Catal. 189 (2000) 370.
[11] F. Figueras, J. Lopez, J. Sanchez-Valente, T.T.H. Vu, J.-M. Clacens, J. Palomeque, J. Catal. 211 (2002) 144.
[12] P.S. Kumbhar, J.S. Valente, J. Lopez, F. Figueras, Chem. Commun. (1998) 535.
[13] P.S. Kumbhar, J.S. Valente, F. Figueras, Chem. Commun. (1998) 1091.
[14] M. Cantu, E. Lopez-Salinas, J.S. Valente, R. Montiel, Environ. Sci. Technol. 39 (2005) 9715.
[15] P.C. Pavan, E.L. Crepaldi, de G.A. Gomes, J.B. Valim, Colloid Surf. A 154 (1999) 399.
[16] P.C. Pavan, G.A. Gomes, J.B. Valim, Micropor. Mesopor. Mater. 21 (1998) 659.
[17] J. Orthman, H.Y. Zhu, G.Q. Lu, Sep. Purif. Technol. 31 (2003) 53.
[18] J. Inacio, C. Taviot-Gueho, C. Forano, J.P. Besse, Appl. Clay Sci. 18 (2001) 255.
[19] R. Celis, W.C. Koskinen, A.M. Cecchi, G.A. Bresnahaw, M.J. Carrioza, M.A. Ulibarri, I. Pavlovic, M.C. Hermosin, J. Environ. Sci. Health B34 (1999) 929.
[20] Y.W. You, H.T. Zhao, G.F. Vance, Appl. Clay Sci. 21 (2002) 217.
[21] L.P. Cardoso, J.B. Valim, J. Phys. Chem. Solids 67 (2006) 987.
[22] A. Legrouri, M. Lakraimi, A. Barroug, A. De Roy, J.P. Besse, Water Res. 39 (2005) 3441.
[23] E.M. Seftel, E. Popovici, M. Mertens, K. De Witte, G.V. Tendeloo, P. Cool, E.F. Vansant, Micropor. Mesopor. Mater. 113 (2008) 296.
[24] A. Patzko, R. Kun, V. Hornok, I. Dekany, T. Engelhardt, N. Schall, Colloid Surf. A 265 (2005) 64.
[25] K. Takagi, T. Shichi, H. Usami, Y. Sawaki, J. Am. Chem. Soc. 115 (1993) 4339.
[26] M.Z. Bin Hussein, Z. Zainal, A.H. Yahaya, A.B.A. Aziz, Mater. Sci. Eng. B 88 (2002) 98.
[27] U. Costantino, N. Coletti, M. Nocchetti, G.G. Aloisi, F. Elisei, Langmuir 15 (1999) 4454.
[28] J. Bauer, P. Behrens, M. Speckbacher, H. Langhals, Adv. Funct. Mater. 13 (2003) 241.
[29] J.S. Valente, E. Lopez-Salinas, M.S. Cantu, F. Hernandez-Beltran, US Patent 2006/0189481 A1 (2006).
[30] L. Zhongqing, Z. Yamping, L. Zhenhua, W. Yichao, G.E. Changchun, Rare Met. 26 (2007) 263.
[31] E. Sánchez, T. López, Mater. Lett. 25 (1995) 271.
[32] M. Alvarez, T. López, J.A. Odriozola, M.A. Centeno, M.I. Domínguez, M. Montes, P. Quintana, D.H. Aguilar, R.D. González, Appl. Catal. B 73 (2007) 34.
[33] F. Rouquerol, J. Rouquerol, K. Sing, Adsorption by Powders and Porous Solids, Academic Press, London, 1999.
[34] C.H. Giles, T.H. MacEwan, S.N. Nakhwa, D. Smith, J. Chem. Soc. (1960) 3973.
[35] F. Tzompantzi, J.S. Valente, M.S. Cantu, R. Gomez, in: S.R. Schmidt (Ed.), Catalysis of Organic Reactions, CRC Press Taylor and Francis Group, Florida, 2007, pp. 55–59.
[36] M.V. Shankar, S. Anandan, N. Venkatachalam, B. Arabindoo, V. Murugesan, Chemosphere 63 (2006) 1014.
[37] M. Lakraimi, A. Legrouri, A. Barroug, A. De Roy, J.P. Besse, J. Mater. Chem. 10 (2000) 1007.
[38] J.I. Pérez-Martínez, J.M. Ginés, E. Morillo, M.L.G. Rodríguez, J.R. Moyano, Environ. Technol. 21 (2000) 209.
[39] K.W. Goyne, J. Chorover, A.R. Zimmerman, S. Komarneni, S.L. Brantley, J. Colloid Interf. Sci. 272 (2004) 10.
[40] H. Chun, W. Yizhong, T. Hongxiao, Chemosphere 41 (2000) 1205.
[41] P.J. Sideris, U.G. Nielsen, Z. Gan, C.P. Grey, Science 321 (2008) 113.
[42] J.A. Gursky, S.D. Blough, C. Luna, C. Gomez, A.N. Luevano, E.A. Gardner, J. Am. Chem. Soc. 128 (2006) 8376.